Design Optimization of Centrifugal Microfluidic "Lab-on-a-Disc" Systems towards Fluidic Larger-Scale Integration

Jens Ducrée

School of Physical Sciences, Dublin City University, Ireland

Abstract

Enhancing the degree of functional multiplexing while assuring operational reliability and manufacturability at competitive costs are crucial ingredients for enabling comprehensive sample-to-answer automation, e.g., for use in common, decentralized "Point-of-Care" or "Point-of-Use" scenarios. This paper demonstrates a model-based 'digital twin' approach which efficiently supports the algorithmic design optimization of exemplary centrifugo-pneumatic (CP) dissolvable-film (DF) siphon valves towards larger-scale integration (LSI) of well-established "Lab-on-a-Disc" (LoaD) systems. Obviously, the spatial footprint of the valves and their upstream laboratory unit operations (LUOs) have to fit, at a given radial position prescribed by its occurrence in the assay protocol, into the locally accessible disc space. At the same time, the retention rate of a rotationally actuated CP-DF siphon valve and, most challenging, its band width related to unavoidable tolerances of experimental input parameters, need to slot into a defined interval of the practically allowed frequency envelope. To accomplish particular design goals, a set of parametrized metrics is defined, which are to be met within their practical boundaries while (numerically) minimizing the band width in the frequency domain. While each LSI scenario needs to be addressed individually on the basis of the digital twin, a suite of qualitative design rules and instructive showcases structures are presented.

Introduction

Empowering even untrained operators to autonomously perform decentralized testing of bioliquids outside specialized laboratory infrastructure, such as hospital labs, general practitioners' offices, in the field, or even patient self-testing at home, represents the key driver for the development of so-called "Point-of-Care" (PoC) devices. While immunochromatographic devices based on lateral flow, e.g., familiar from blood glucose or pregnancy testing, have been around for several decades, aging populations, the rise of chronic and life-style related diseases correlating with increasing age, wealth, nutritional habits and sedentary lifestyles of global populations, or recent pandemic threats, create a dire need for frequent, ubiquitous, simple, reliable, cost-efficient and user-friendly monitoring of biochemical indicators in various body fluids. Similar local testing capabilities are also desirable for often quasi-continuous point-of-use ("PoU") or at-line monitoring of industrial processes, infrastructures and the environment.

Since their emergence the early 1990s [1-7], microfluidic Lab-on-a-Chip technologies, often quite synonymously referred to as micro Total Analysis Systems ("µTAS"), have been touted a highly promising candidate to provide compact and inexpensive devices offering full sample-to-answer automation of multiplexed bioassay protocols. Over the recent decades, manifold platform technologies have been established, which might be categorized by their pumping, valving, actuation, manufacturing, assay or detection schemes. The field has substantially diversified in the meantime,

40 and many, mostly application-specific solutions, have been successfully advanced to wealth of
41 demonstrators and an increasing number of viable products.

42 Due to their plain concept of flow control by a simple spindle motor and its analogies to, at the time,
43 booming optical data storage technologies such as CD and DVD, centrifugal microfluidic systems [8-
44 37] have been one of the earliest microfluidic platforms to be developed, starting around the mid-
45 1990s [8-10, 13, 14, 38, 39]; interestingly, these "Lab-on-a-Disc" (LoaD) systems, which conceptually
46 resemble conventional centrifugal analyzers, were first commercialized before finding their way into
47 academia around the turn of the millennium. By now, a sizable, global cohort of companies and
48 research groups has been involved in advancing and maturing LoaD technologies [10, 13, 40-46].

49 Note that, for the sake of simplicity, we use the term "disc" throughout this paper; however, a plethora
50 of geometries, e.g., minidiscs, segments, microscope slides or tubes, which substantially deviate from
51 the standard format of conventional optical data storage media displaying 12-cm (outer), 1.5 cm (inner
52 hole) diameter and 1.2-mm thickness, have been introduced. Furthermore, different mounting
53 concepts to the axis of rotation have been implemented. Yet, centrifugal flow control only depends
54 on the radial position and the (square of the) spin rate, while not depending on the particular shape
55 of the carrier chip and its mode of attachment to the spindle.

56 By virtue of the ubiquitous and unidirectional centrifugal field acting simultaneously on all liquids
57 loaded to their potentially fast spinning device, valving concepts play a paramount role in LoaD
58 technologies. While there have been active modes of control, e.g., by co-rotating pumps [47, 48] or
59 sacrificial barriers [49-51] opened by stimuli delivered by instrument mounted external units, or
60 release of stored chemical energy [52], rotationally actuated schemes have attracted distinct attention
61 due to their smooth alignment with the low complexity concept of LoaD platforms with their rugged
62 instrument "playing" a mostly single-use disc cartridge.

63 In most LoaD systems, these valves retain the liquid during so-called laboratory unit operations
64 ("LUOs"), such metering and mixing, as extensively covered in the literature [48, 53-72], and briefly in
65 a subsequent section within the context of LSI. Furthermore, while essential ingredients for full-
66 fledged LoaD applications, we refer to the numerous specialized publications regarding the many,
67 primarily optical or electrochemical, techniques for downstream detection [18-37, 73, 74].

68 In traditional valving mechanisms, the spinning-induced pressure head, which simultaneously acts on
69 all disc-based liquid volumes, is opposed by different sources of counterpressure. For instance,
70 interfacial tension is at the root of capillary burst valves; liquids are retained in siphon valves until the
71 capillary pressure exceeds the centrifugal pressure by lifting [14], lowering [9] or accelerating [75] the
72 spin rate across critical frequency thresholds, or overflow prompted by volume addition under
73 prevalent artificial gravity conditions.

74 This work runs along the example of centrifugo-pneumatic (CP) dissolvable-film (DF) siphon valving
75 that has shown to offer wide tunability, configurability, and operational robustness compared to other
76 rotationally controlled valving schemes [31, 35, 75-77]. Yet, the portrayed digital twin method [78-
77 80], i.e., the model-based virtual representation of a physical object or process, can readily be
78 extended to characterize and refine other flow control mechanisms over their multidimensional
79 parameter spaces.

80 This paper investigates systematic design optimization of rotationally actuated valves to facilitate
81 fluidic large(r)-scale integration (LSI). The notion of microfluidic LSI has first elaborated in the early
82 2000s in the context of pneumatically controlled elastomeric systems [81]. Based on previous
83 publications on 'digital twin' [80] modelling of fluidic performance and operational robustness on

84   LoaD systems [76, 82], valve retention frequencies and their band widths were identified as key
85   performance indicators, and can directly be calculated, either algebraically of numerically, from the
86   standard deviation of elementary input parameters, such as general (linear) machining and pipetting
87   tolerances [83, 84].

88   These statistical spreads can either be found in manuals or the literature, or be determined by low-
89   complexity test structures; importantly, these basic parameters are broadly independent of the
90   specific layout of a specific LoaD cartridge. This method is hence essential to predict and optimize
91   device performance and its operational robustness *in-silico*, prior to the time- and resource-
92   consuming, and thus risky and costly development of manufacturing and assembly. Such facilities are
93   rarely available in academic labs, and not even during early-stage research and development projects
94   in common industrial environments.

95   At first, the principles of centrifugal flow control are modelled to support a digital twin of LoaD systems
96   orchestrated by a group of CP-DF siphon valves. Then, fundamental requirements underlying
97   rotational valving for fluidic LSI in real and frequency space are elaborated. In the next section, a set
98   of performance metrics supporting the initial, knowledge-based qualitative design and its subsequent,
99   computational optimization are defined. Examples for typical tasks in multiplexing and resulting valve
100 geometries are given before compiling general rules guiding the layout and rotational automation of
101 multi-step / multi-reagent bioanalytical assay panels.

Rotational Flow Control

103 ### Pressures
104 A (contiguous) fluid segment of volume U_0 and density ϱ possessing a radial extension $\Delta r = r - r_0$
105 and mean radial position $\bar{r} = 0.5 \cdot (r + r_0)$ between its inner and outer menisci r and r_0, respectively,
106 which resides in a valve of (static) geometry Γ experiences a centrifugal pressure head

$$p_\omega = \varrho \cdot \bar{r} \Delta r \cdot \omega^2 \qquad (1)$$

107 when spinning at an angular frequency $\omega = 2\pi \cdot \nu$. Given typical experimental values, e.g., $\varrho = $
108 $10^3 \, \text{kg m}^{-3}$, $\bar{r} = 3 \, \text{cm}$, $\Delta r = 1 \, \text{cm}$, lower elevated spin rates $\nu = \omega/2\pi = 10 \, \text{Hz}$ and $50 \, \text{Hz}$,
109 equation (1) yields $p_\omega \approx 12 \, \text{hPa}$ and $300 \, \text{hPa}$, respectively. So even the larger value of p_ω (13) only
110 induces roughly one third of the standard atmospheric pressure $p_{\text{std}} = 1013.25 \, \text{hPa}$.

111 Additional pressures $p_\rightarrow$ and $p_\leftarrow$ may act on the fluid, which are directed parallel or against the main
112 z-axis of a channel, respectively. The pneumatic pressure

$$p_V = p_0 \cdot \frac{V_0}{V} \qquad (2)$$

113 results from the compression of an original gas volume V_0 initially held at ambient pressure p_0 to V
114 (law of Boyle-Mariotte). Theoretically, p_V (2) can be made arbitrarily large through sufficiently
115 shrinking the final volume V (for a static V_0 defined by Γ). Note that, in addition to the compressibility,
116 a volume-pressure relationship akin to (2) can also arise in fluidic systems containing flexible solid
117 elements such as elastic lids or membranes [30]. The base pressure p_0 may also be modified by heating
118 or cooling [62] according to $V \propto T$ (Charles's law).

119 A capillary pressure

$$p_\Theta = \frac{4\sigma}{D} \cdot \cos\Theta \qquad (3)$$

120 is exerted on a liquid of surface tension σ with a contact angle Θ to a (cylindrical) channel of diameter
121 D. For water with $\sigma \approx 72.8 \times 10^{-3} \, \text{N m}^{-1}$, and a hydrophobic contact angle $\Theta \approx 120°$
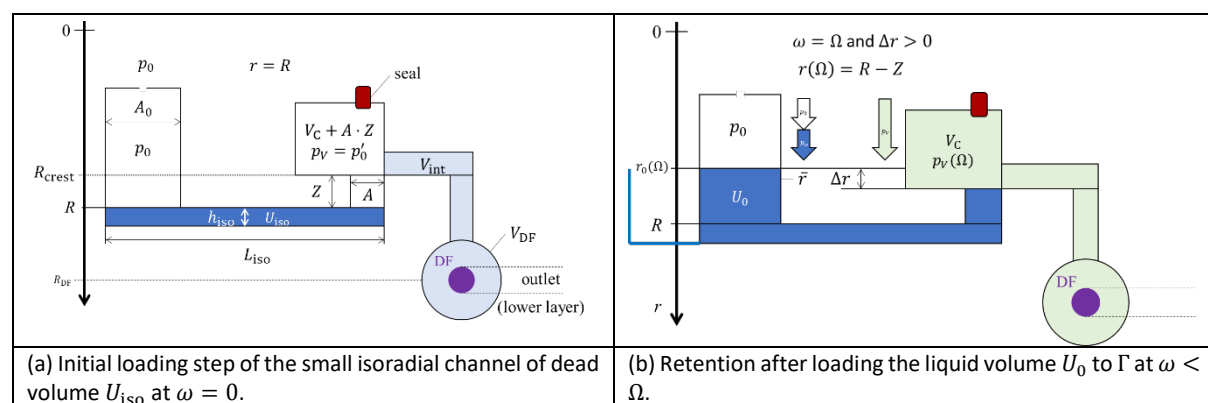
122   (approximately corresponding to a Teflon coating in contact with aqueous) in a conduit with $D =$
123   $100\,\mu m$, the capillary counterpressure amounts to $|p_\Theta| \approx 15\,\text{hPa} \ll p_{\text{std}}$, only, which would be
124   matched by rather low spin rates in the region $\nu = \omega/2\pi \approx 10\,\text{Hz}$. In refined models, also pressures
125   resulting from the viscosity- and geometry-dependent hydrodynamic resistance (law of Hagen-
126   Poiseuille), the deceleration of flow or inertial agitation of liquid samples and reagents driven by $r \cdot$
127   $d\omega/dt$ ought to be factored in.

128   In hydrostatic equilibrium

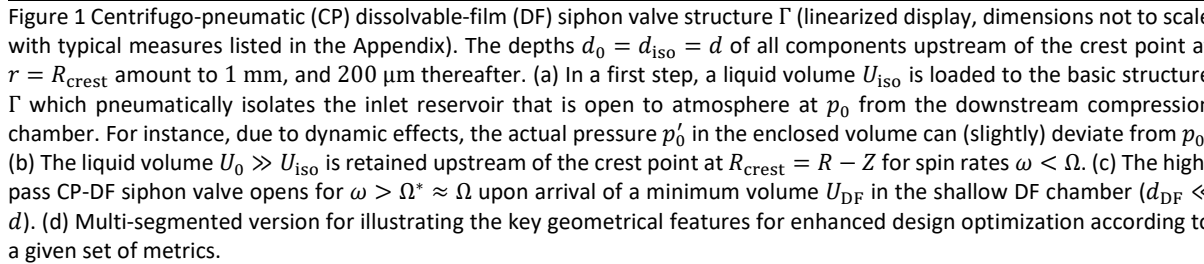$$p_\omega + p_\rightarrow = p_\leftarrow \tag{4}$$

129   a liquid distribution $\Lambda = \Lambda(\omega)$ stabilizes within a given geometry Γ in response to p_ω (1), $p_\rightarrow$ and $p_\leftarrow$,
130   e.g., p_V (2) or p_Θ (3). The outer meniscus $r = r(\omega)$ is a function of ω, and r_0 can then be directly
131   determined for a given Γ and U_0.

Critical Spin Rate

133   During retention of rotationally actuated valves, the outer meniscus of Λ at $r(\omega)$ remains upstream
134   of a critical filling level marked by a defined position Z along the axial direction z of the structure Γ. In
135   case $p_\rightarrow$ and $p_\leftarrow$ do not (explicitly) depend on ω, combining (1) and (4) leads to a retention rate

$$\Omega = \Omega(U_0, \Gamma, z = Z) = \sqrt{\frac{p_\leftarrow - p_\rightarrow}{\varrho \cdot \bar{r}\Delta r}} \tag{5}$$

136   beyond which the liquid is released at $\omega > \Omega$ and $\omega < \Omega$ for high- and low-pass valves, respectively.
137   For the sake of clarity, we focus on high-pass valves in the following.

Example: Centrifugo-Pneumatic Siphon Valves

139   In prior publications, we have compared different rotationally actuated valving schemes for LoaD
140   systems through a more general digital twin approach [76, 82]. It turns out that normally-closed
141   centrifugo-pneumatic (CP) siphon valves with a compression chamber of volume V_C that is initially
142   sealed by dissolvable-film (DF) membrane offer many operational benefits; amongst them are wide
143   tunability of the critical spin rate Ω (5), high operational robustness, and flexible configurability in real
144   space as well as in the frequency domain.

(a) Initial loading step of the small isoradial channel of dead volume U_{iso} at $\omega = 0$.

(b) Retention after loading the liquid volume U_0 to Γ at $\omega < \Omega$.

| (c) Liquid release at $\omega > \Omega$ after a sufficient volume $U_{DF} \gg U_{iso}$ has arrived in the DF chamber, i.e., $\omega = \Omega^*$. | (d) Refined, multi-segmented layout for refined design optimization during liquid retention $\omega \leq \Omega$. |

Figure 1 Centrifugo-pneumatic (CP) dissolvable-film (DF) siphon valve structure Γ (linearized display, dimensions not to scale with typical measures listed in the Appendix). The depths $d_0 = d_{iso} = d$ of all components upstream of the crest point at $r = R_{crest}$ amount to 1 mm, and 200 µm thereafter. (a) In a first step, a liquid volume U_{iso} is loaded to the basic structure Γ which pneumatically isolates the inlet reservoir that is open to atmosphere at p_0 from the downstream compression chamber. For instance, due to dynamic effects, the actual pressure p_0' in the enclosed volume can (slightly) deviate from p_0. (b) The liquid volume $U_0 \gg U_{iso}$ is retained upstream of the crest point at $R_{crest} = R - Z$ for spin rates $\omega < \Omega$. (c) The high-pass CP-DF siphon valve opens for $\omega > \Omega^* \approx \Omega$ upon arrival of a minimum volume U_{DF} in the shallow DF chamber ($d_{DF} \ll d$). (d) Multi-segmented version for illustrating the key geometrical features for enhanced design optimization according to a given set of metrics.

Figure 1 illustrates the basic operating principle of a CP-DF siphon valving structure Γ located at a radial position R with respect to the axis of rotation at $r = 0$. In a (hypothetical) priming procedure, a liquid volume U_{iso} is first loaded to completely fill the tiny isoradial channel; as a result, a gas volume V_0 composed of a main compression chamber of volume $V_{C,0}$, an inbound segment of volume $A \cdot Z$, and tiny outlet features with negligible volume contributions $V_{out}/V_0 \ll 1$ is cut off from the inlet that is open to atmosphere at p_0 (Figure 1a, typical dimensions in the Appendix). The actual pressure p_0' in the enclosed gas might deviate from the ambient pressure p_0, e.g., due to filling dynamics. Then, the remainder of U_0 is added to the open inlet reservoir. At the retention rate $\omega = \Omega$, the outer meniscus has progressed in the radially inbound section of cross section A and axial length Z to the crest point at $R_{crest} = R - Z$ (Figure 1b).

This high-pass, CP-DF siphon valve opens above $\omega = \Omega$ once sufficient liquid U_{DF} has entered the outer chamber to cover the local DF membrane at R_{DF} (Figure 1c). Strictly speaking, there is a release rate $\Omega^* > \Omega$ needed for displacing U_{DF} from the inbound section terminated at R_{crest} into the outer chamber to open the valve. This offset is usually very small and can be calculated from (5) by substituting U_0 by $U_0' = U_0 - U_{DF}$; for the sake of simplicity, and unless otherwise mentioned, we assume $\Omega^* \approx \Omega$. Figure 1d displays a multi-segmented design of the core structure Γ used later for advanced optimization.

Inserting $p_\rightarrow = p_0$ and $p_\leftarrow = p_V$ (2), we obtain

$$\Omega = \sqrt{\frac{p_0 \cdot (V_C/V - 1)}{\varrho \cdot \bar{r}\Delta r}} \tag{6}$$

for the critical retention rate Ω (5) of CP-DF siphon valves with $V = V_C - A \cdot Z$.

Operational Robustness

The critical frequencies Ω (5, 6) of rotationally controlled valves depend on a number of parameters $\{\gamma_k\}$, such as the loaded liquid volume U_0 (its density ϱ is fairly constant for aqueous solutions at room temperature), the structural dimensions of Γ, and the quantities determining the contributing pressure contributions (1), (2) and p_0. Experimentally, each input parameter γ_k is thus displays a

178 normal distribution of standard deviation $\Delta\gamma_k$. Consequently, also the resulting critical spin rate Ω (5)
179 displays a spread

$$\Delta\Omega \approx \sqrt{\sum_k \left(\frac{\partial\Omega}{\partial\gamma_k} \cdot \Delta\gamma_k\right)^2} \qquad (7)$$

180 as approximated by Gaussian error propagation, assuming small $\{\Delta\gamma_k\}$ and mutually independent
181 $\{\gamma_k\}$. Operationally robust valving can thus only be assured if the spin rate ω is moved across the
182 frequency band $\Omega \pm M \cdot \Delta\Omega$; the factor M determines the level of functional robustness P_M evaluated
183 by $1 - \text{erf}\,[M/\sqrt{2}]$ with the error function "erf"; so, for $M \in \{1,2,3,4,\dots\}$, valving reliability can be
184 gauged at $P_M \approx \{68\%, 95\%, 99.7\%, 99.99\%, \dots\}$.

Laboratory Unit Operations

186 Common bioanalytical assay panels are automated on most LoaD platforms by batch-wise "stop-and-
187 go" processing. To this end, the bioanalytical protocols are dissected into laboratory unit operations
188 (LUOs), each of them controlled by normally closed valve. Centrifugally implemented LUOs have been
189 covered extensively in the literature, e.g., for metering / aliquoting [60-62], resuspension of dry and
190 mixing with liquid reagents [63-66], incubation, purification / concentration / extraction [48, 67],
191 homogenization [68, 69], particle filtering [53-59], and droplet generation [70-72].

192 From a fluidic point of view, each LUO is typically implemented by the interplay of a spin protocol
193 $\omega(t)$, possibly featuring steeper ramps $d\omega/dt$, with a specifically shaped chamber upstream of the
194 valve. For the important LUO of plasma separation, a minimum field strength

$$f_\omega = \Delta\varrho \cdot \mathcal{R} \cdot \omega^2 \qquad (8)$$

195 is required to act on particles (or volume elements) of differential density $\Delta\varrho$ with respect to their
196 suspending (liquid) medium at radial position $\mathcal{R}$. For allowing proper operation of the rotationally
197 actuated (high-pass) valve at its outlet, $\omega(t) < \Omega$ must be observed.

Design Optimization

Multiplexing

200 The sample-to-answer automation of bioanalytical protocols representing comprehensively
201 parallelized, multi-analyte assay panels including elements like calibrants, redundancies and dilution
202 series, is enabled by fluidic larger-scale integration (LSI) in the backend [82]. Towards high packing
203 densities, each valve design Γ_i hence needs to curtail their footprint in the radial, aerial and frequency
204 domain, while concurrently meeting additional requirements, such as allowing a certain field strength
205 f_ω (8) to assure proper execution of its upstream LUO.

206 A typical task in fluidic LSI of LoaD systems is thus to tailor a valve structure Γ_i for fitting into
207 unoccupied radial and azimuthal intervals at the radial location R while squeezing the band $\Omega_i \pm M \cdot$
208 $\Delta\Omega_i$ associated with the standard deviations $\{\Delta\gamma_k\}$ of its impact parameters $\{\gamma_k\}$ into a still empty ω-
209 corridor.

Parameter Space

211 The radial space $R_{\min} < r < R_{\max}$ practically available for placing the valving structures $\{\Gamma_i\}$ is
212 confined between the minimum and maximum structurable and bondable positions $R_{\min}$ and $R_{\max}$
213 inside the surface of the disc radius. There might be further boundary conditions for the parameters
214 $\{\gamma_k\}$ and resulting geometrical features of Γ_i, e.g., on minimum and maximum dimensions, adequate

215   wall thicknesses, bending radii, draft angles, contact surface, and aspect ratios related to
216   manufacturing and assembly.

217   The upper boundary $\omega_{\max}$ of the frequency envelope, within which LoaD can be operated, is limited
218   by factors like the maximum torque of the spindle motor, the aerodynamic drag of the LoaD cartridge
219   and its rotor, the pressure tightness of the chip assembly, and safety concerns. There may also be a
220   lower limit $\omega_{\min}$, e.g., required to broadly suppress uncontrolled capillary flow by a dominant
221   centrifugal pressure $p_\omega \propto \omega^2$ (1), which is roughly achieved in the range $\omega > 10$ Hz, see back of the
222   envelope calculation in the context of p_Θ (3). Thus, there is only a finite ω-space available for the
223   bands $\{\Omega_i \pm M \cdot \Delta\Omega_i\}$ associated with the (joint) critical spin rate $\{\Omega_i\}$ (5,6) of each independently
224   operated bunch of valves.

225   While the use of disc space is mainly linked to the geometry Γ and its radial position R, the tolerances
226     $\{\Delta\gamma_k\}$ in the experimental parameters $\{\gamma_k\}$ sensitively affect the band width $2 \cdot M \cdot \Delta\Omega$ (7). Guidelines
227   for the systematic minimization of the standard deviation $\Delta\Omega_i = \Delta\Omega_i(\{\gamma_k, \Delta\gamma_k\})$ will thus play a
228   pivotal role in the subsequently discussed design optimization.

Performance Metrics / Criteria

230   This section presents a suite of metrics $\{\mathcal{M}_l\}$ to be minimized in order to accomplish specific design
231   goals towards fluidic LSI. Each of these metrics $\{\mathcal{M}_l\}$ depends on several (experimental) parameters
232     $\{\gamma_k\}$ and their standard deviations $\{\Delta\gamma_k\}$, i.e., $\mathcal{M}_l = \mathcal{M}_l(\{\gamma_k, \Delta\gamma_k\})$. By convention, these metrics
233     $\{\mathcal{M}_l\}$ are defined here to vanish towards the targeted design goal, and approach unity for its largest
234   (practical) value, i.e., $0 \leq \mathcal{M}_l \leq 1$. Design optimization of a given structure Γ_i according to a metric
235     $\mathcal{M}_l$ thus comes down to their minimization in multidimensional space constituted by the variables
236     $\{\gamma_k, \Delta\gamma_k\}$.

237   Geometries Γ_i derived in isolation, i.e., from reducing a single metric $\mathcal{M}_l$, tend to have very
238   questionable benefit towards LSI. For example, a minimum spatial footprint may be associated with a
239   band width $\Omega_i \pm M \cdot \Delta\Omega_i$ of the same magnitude as the entire ω-corridor, thus detrimentally
240   undermining multiplexing. In the examples presented, we commonly optimize the metrics $\mathcal{M}_l$ while
241   concurrently keeping the standard deviation $\Delta\Omega_i$ at bay.

242   In theory, the entire (available) multiparameter space $\{\gamma_k\}$ must be probed for a given $\{\Delta\gamma_k\}$ to spot
243   the absolute minimum of $\mathcal{M}_l$, which would commonly require enormous computational power.
244   Efficient numerical algorithms rather seek local minima by following the steepest local (downward)
245   slope. By choosing, either statistically, or via a clever educated guess, a favorable starting point, a
246   sufficiently small value for $\mathcal{M}_l$ may still be identified. In practice, convergence of the numerical
247   methods within reasonable boundaries in multidimensional parameter space $\{\gamma_k, \Delta\gamma_k\}$ involves
248   iterative "hinting" of promising initial locations to the program. Therefore, the subsequently
249   calculated structures Γ might not represent absolute minima of the target metric(s) $\mathcal{M}_l$; they rather
250   provide instructive design guidelines that can be further refined.

251   Component- and device-level optimization of a valving structure Γ usually needs to consolidate an
252   array of possible contradictory demands, e.g., on minimum field strength f_ω (8), radially outbound
253   staggering of LUO-valve for serial processing, non-overlapping stacking bands $\{\Omega_i \pm M \cdot \Delta\Omega_i\}$ (7), and
254   the surface area required for holding volumes of compression chambers V_C, liquid samples and
255   reagents $\{U_{0,i}\}$ imposed by the assay protocol. We thus discuss the concept of multi-parameter
256   optimization in the final subsection.

Band Width

257   The operational robustness of rotationally controlled valves correlates with their standard deviation
259   $\Delta\Omega$ (7) of their critical spin rate Ω (5). This spread varies with the parameters $\{\gamma_k\}$ like R, U_0 and p_0,
260   the dimensions delineating in the geometry Γ, and their tolerances $\{\Delta\gamma_k\}$ mainly owing to precision
261   of manufacturing, assembly, liquid metering and the ambient pressure p_0. For a CP-DF siphon valve
262   with default geometry Γ (Figure 1), the dependency of $\Delta\Omega$ on the compression volume $V_{C,0}$ with
263   common geometrical manufacturing tolerances $\Delta\gamma_k$ (Appendix), and the precision of the loaded liquid
264   volume ΔU_0 is displayed in Figure 2. Accordingly, if disc space and radial ordering allows, it is favorable
265   to enlarge the (primary) volume $V_{C,0}$ compression chamber until the curve saturates (Figure 2a), and
266   to move Γ to outer radial positions R (Figure 2b).

(a) $\Delta\Omega/2\pi$ vs. volume of the main compression chamber $V_{C,0}$ of Γ with $R = 3$ cm.

(b) $\Delta\Omega/2\pi$ vs. the radial position R of Γ with $V_{C,0} = $ const.
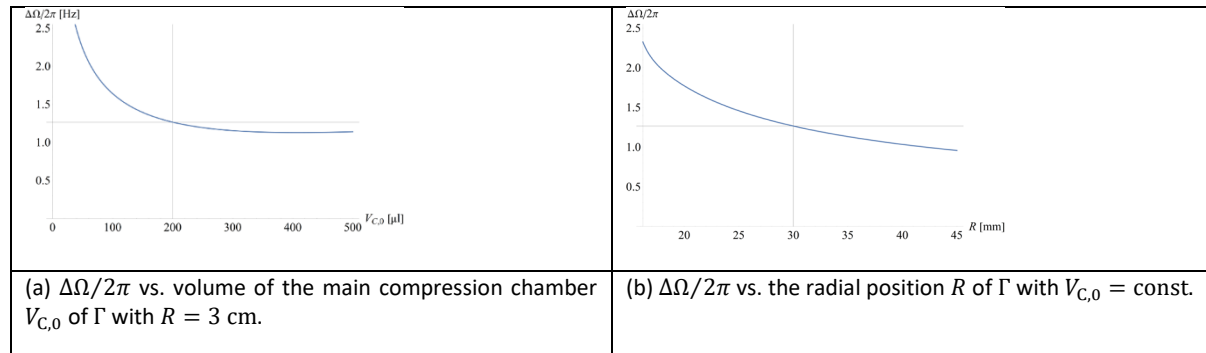
267   Figure 2 Standard deviation $\Delta\Omega/2\pi$ for CP-DF siphon valves (with default parameters, see Appendix) as a function of (a) the
268   volume of the main compression chamber $V_{C,0}$, and (b) the radial position R for typical dimensional (manufacturing)
269   tolerances (see Appendix). The dotted horizontal and vertical lines indicate the standard deviation of Ω and the volume of
270   main compression chamber $V_{C,0}$ in the default geometry and parameters.

271   As already pointed out, the band width $\Delta\Omega$ (7) assumes a pivotal role in directing the layout of
272   fluidically multiplexed centrifugal microfluidic LoaD systems. Common optimization tasks of valving
273   structures Γ in multiplexed liquid handling scenarios are thus often intertwined with restricting the
274   spread $\Delta\Omega$ of each valving step. We introduce the normalized metric

$$\overline{\Delta\Omega} = \frac{\Delta\Omega}{\omega_{\max} - \omega_{\min}} \tag{9}$$

275   for its computational minimization by a wide range of well-established numerical routines that is
276   available in widely available software packages.

Refined Geometry

278   In order to improve options for reducing $\Delta\Omega$ (7), or $\overline{\Delta\Omega}$ (9), we have advanced the plot of the valve Γ
279   by compartmentalizing its most critical segments (Figure 1d). Figure 3 discloses that the increased
280   number of dimensions in the parameters space γ_k permit lowering the spread $\Delta\Omega/2\pi$ from 0.95 Hz
281   to 0.86 Hz for the same $R = 3$ cm and release rate $\Omega/2\pi \approx 25$ Hz. For $M = 4$, this would correspond
282   to a trimming the band width $M \cdot \Delta\Omega/\pi$ from 5.70 Hz to 5.16 Hz. A further cut in $\Delta\Omega$ is expected for
283   more challenging cases, e.g., for enabling elevated retention rates Ω (5,6).
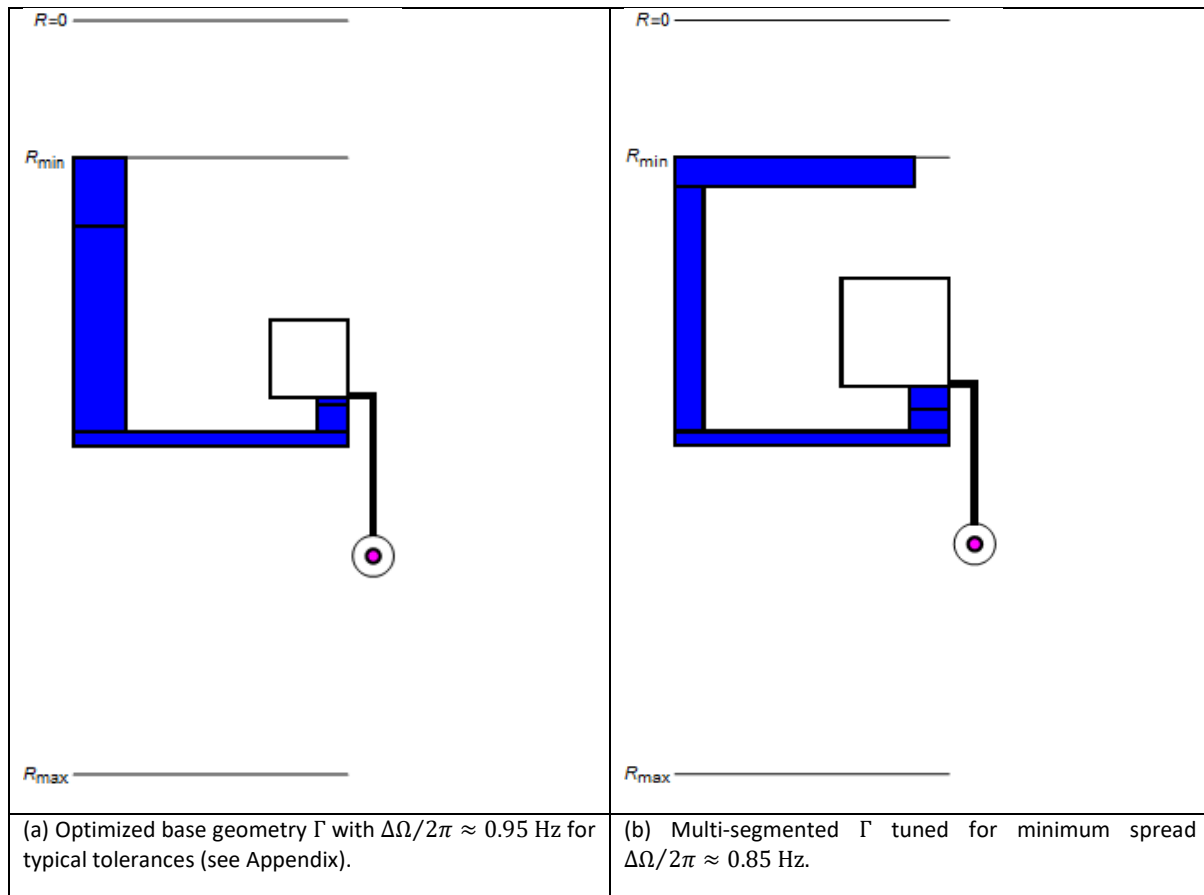
| (a) Optimized base geometry Γ with $\Delta\Omega/2\pi \approx 0.95$ Hz for typical tolerances (see Appendix). | (b) Multi-segmented Γ tuned for minimum spread $\Delta\Omega/2\pi \approx 0.85$ Hz. |

Figure 3 Comparison between structures Γ in their (a) basic and (b) multi-segmented versions for typical tolerances $\{\Delta\gamma_k\}$ (see Appendix) at identical radial position $R = 3$ cm and release rate $\Omega/2\pi = 25$ Hz after optimization of $\Delta\Omega$. Most notably, Γ in (b) displays a wider inner radial section of the reservoir and overall increased width of the inbound segment to "pin" the menisci at r_0 and $r = R_{\text{crest}}$, and thus $\bar{r}\Delta r$, to counter variation in Ω (5,6) via $\bar{r}\Delta r$.

Retention Rate and Field Strength

Liquids loaded to high-pass valves (Figure 1) are held back for $\omega < \Omega \propto (\bar{r}\Delta r)^{-1/2}$ (5); considering that $\bar{r}$ closely relates to the distance from the center of rotation $r = R$, the structure Γ may be configured for a given liquid volume U_0 (exceeding the dead volume of Γ outside R_{crest}) to minimize the difference in liquid levels Δr between the inlet reservoir and the radially inbound section; at least mathematically, Ω (5) can then be tuned to any arbitrarily high value.

For the specific case of CP-DF siphon valves (Figure 1) primarily investigated here, the scaling $\Omega \propto (V_C/V - 1)^{1/2}$ (6) reveals that Ω also increases with the compression ratio V_C/V between the initial and the final volumes V_C and V of the enclosed gas pocket, respectively. However, especially minimizing the compression volume V_C, or the liquid level difference Δr (not shown), entails a sharply increasing $\Delta\Omega$ (Figure 2a). Hence, in most cases, maximizing the retention rate Ω (5) needs to be carried out while confining $\Delta\Omega$ (7) to reasonable territories in ω-space.

As a typical LUO requiring maximization of Ω while limiting $\Delta\Omega$ for compatibility with fluidic LSI, we look at the centrifugal sedimentation which is governed by the field strength $f_\omega = \Delta\varrho \cdot R \cdot \Omega^2$ (8) experienced by a particle of density differential $\Delta\varrho$ with respect to the suspending medium at the radial position R and retention rate Ω. The metric

$$\bar{f}_\omega = \frac{R \cdot \Omega^2}{R_{\max} \cdot \omega_{\max}^2} \tag{10}$$

may be used for optimizing the field strength f_ω on a disc. In many cases, $R \approx R$.

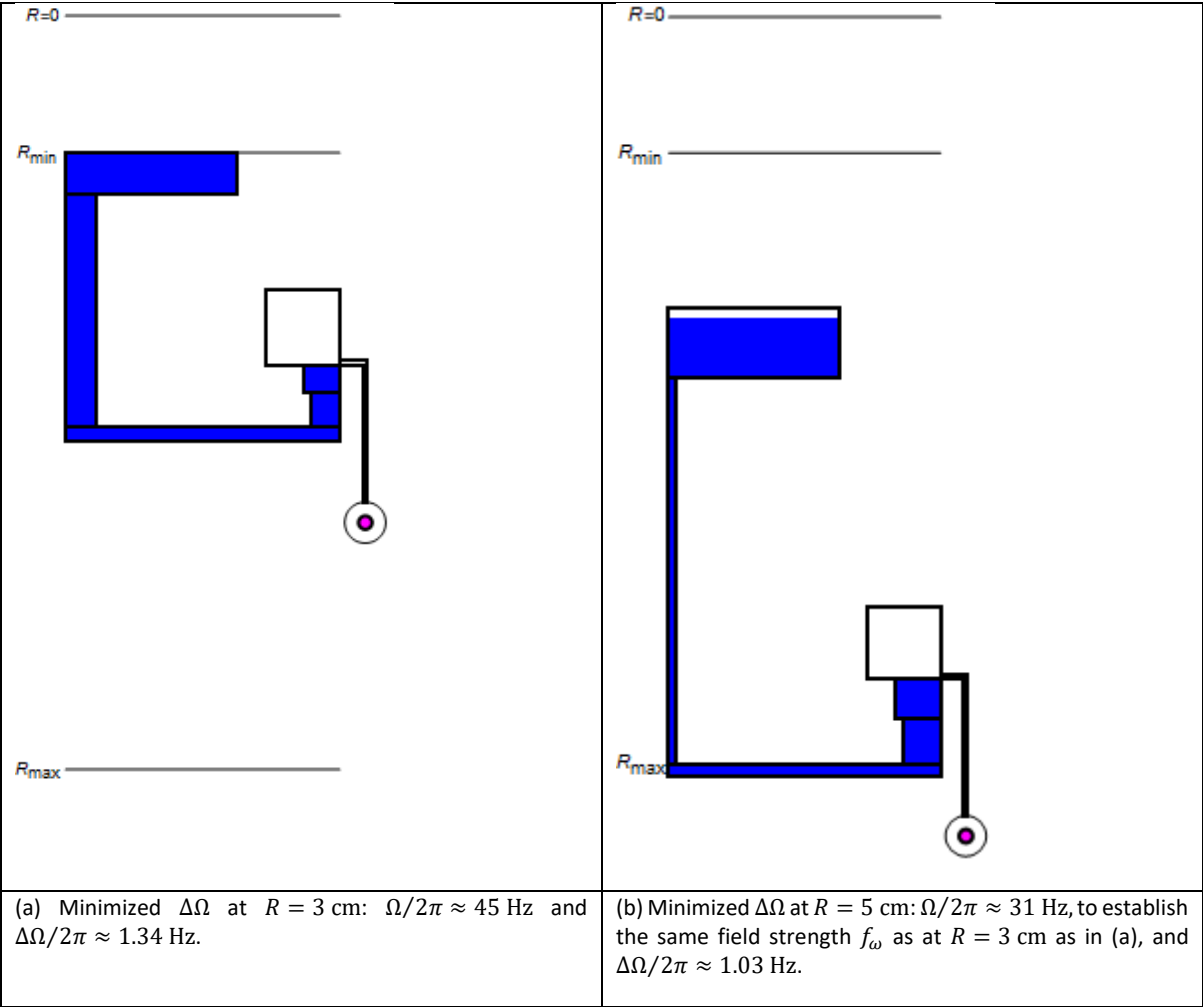| (a) Minimized $\Delta\Omega$ at $R = 3$ cm: $\Omega/2\pi \approx 45$ Hz and $\Delta\Omega/2\pi \approx 1.34$ Hz.	(b) Minimized $\Delta\Omega$ at $R = 5$ cm: $\Omega/2\pi \approx 31$ Hz, to establish the same field strength f_ω as at $R = 3$ cm as in (a), and $\Delta\Omega/2\pi \approx 1.03$ Hz.

Figure 4 (a) Optimizing the band width at (a) $R = 3$ cm and $\Omega/2\pi = 40$ Hz with $\Delta\Omega/2\pi \approx 1.34$ Hz and (b) at $R = 5$ cm by reducing Ω to establish the same field strength $f_\omega \propto R \cdot \Omega^2$ (8), with $\Delta\Omega/2\pi \approx 1.03$ Hz.

Figure 4 reveals how the multi-segmented structure Γ (Figure 1d) can be adjusted to minimize $\Delta\Omega$ while providing the same field strength f_ω (8) at both (representative) radial locations $R = 3$ cm (a) and 5 cm (b). Such a design task may occur if the location of the particle sedimentation needs to be radially shifted, for instance, towards the center, to occur at an earlier stage of a serial liquid handling sequence, or to be placed where space is more ample in the outer region of the disc.

Concurrent Valving

For their simultaneous rotational actuation, valves ideally share the same Ω to save precious ω-space. However, it may often be necessary to place their structures $\{\Gamma_i\}$ at the different radial position $\{R_i\}$. Figure 5 illustrates how Γ is altered at inner and (extreme) outer locations $R = 3$ cm (a) and 5.5 cm (b) to minimize $\Delta\Omega$ while maintaining the same $\Omega/2\pi = 25$ Hz.

| (a) $R = 3$ cm, $\Omega/2\pi \approx 25$ Hz: $\Delta\Omega/2\pi \approx 0.86$ Hz. | (b) $R = 5.5$ cm, $\Omega/2\pi \approx 25$ Hz: $\Delta\Omega/2\pi \approx 0.83$ Hz. |
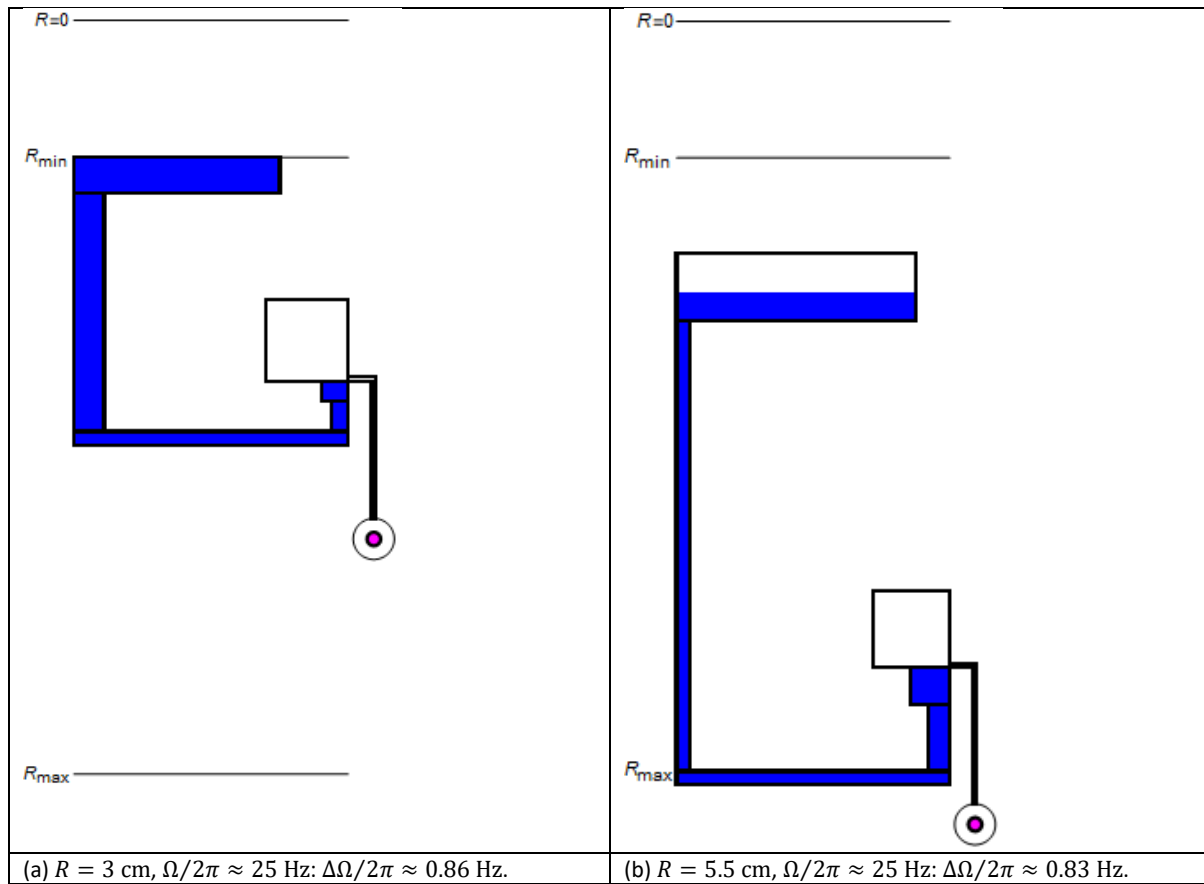
317   Figure 5 Minimization of the standard deviation $\Delta\Omega$ for a set of CP-DF siphon valves Γ possessing equal retention rates
318    $\Omega/2\pi = 25$ Hz, which are placed the radial positions (a) $R = 3$ cm and (b) $R = 5.5$ cm.

319   ## Radial Space

320   Factoring in the finite spacing between $R_{\min}$ and $R_{\max}$, and the need for outbound staggering of
321   serially executed LUOs, valving structures Γ should also be taxed by the metric

$$\bar{R} = \frac{R - \min[r_0(\omega)]}{R_{\max} - R_{\min}} \tag{11}$$

322   for the radial interval they cover between their inner- and outermost confinements $r_0(\omega)$ in the inlet
323   and R (neglecting $d_{\mathrm{iso}} \ll R$) of Γ, respectively (Figure 1a). Figure 6 displays structures Γ that have
324   been optimized for consuming a minimum radial interval $\bar{R}$ (11) at $R = 3$ cm (a) and 5 cm (b).

(a) Radial footprint $\overline{\Delta R}$ of Γ reduced to 1.8 cm at $R = 3$ cm with $\Delta\Omega\,/2\pi \approx$ 0.87 Hz.	(b) Radial footprint $\overline{\Delta R}$ of Γ reduced to 1.8 cm at $R = 5$ cm with $\Delta\Omega\,/2\pi \approx$ 0.95 Hz.	(c) Minimization of areal footprint $\bar{A}$ (excluding compression chamber) with of $\Delta\Omega/2\pi \approx 0.86$ Hz.
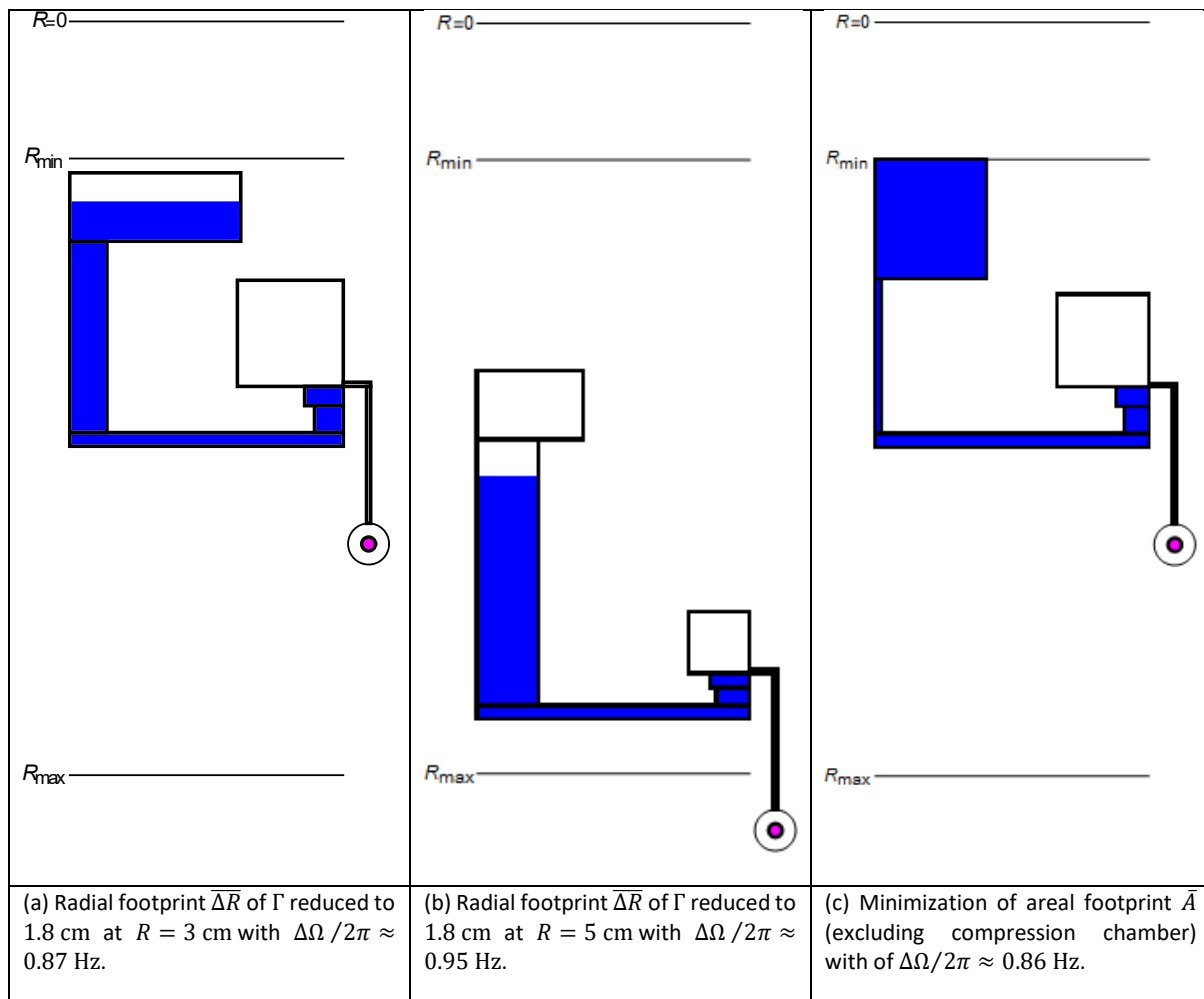
Figure 6 Geometrical optimization of Γ towards minimization of $\Delta\Omega$ at a given $\Omega/2\pi = 25$ Hz towards minimum radial extension $\overline{\Delta R}$ (11) at the radial positions (a) $R = 3$ cm, (b) $R = 5$ cm, and (c) towards smallest spatial footprint $\bar{A}$ (13) at $\Omega/2\pi \approx 25$ Hz. (c)

Furthermore, LUOs that are run early in the protocol, e.g., particle sedimentation or initial metering of loaded liquids, may need to be placed more centrally in order to allow radially outbound staggering of subsequent process steps within the interval $R_{\min} \leq \min[r_0(\omega)] < R_{\mathrm{crest}} \leq R_{\max}$. The metric

$$\check{R} = \frac{R - R_{\min}}{R_{\max} - R_{\min}} \tag{12}$$

can then be minimized to favor the placement of Γ near the center of rotation at $r = 0$. However, especially for LUOs requiring high field strength f_ω (8), this comes at the expense of a larger band width $\Delta\Omega$ (see also Figure 2b).

Spatial Footprint

Owing to the rotational symmetry of LoaD systems, overall disc space $\pi \cdot (R_{\max}^2 - R_{\min}^2)$ is scarce. We define the metric

$$\bar{A} = \frac{A_\Gamma}{\pi \cdot (R_{\max}^2 - R_{\min}^2)} \tag{13}$$

which relates the total surface area A_Γ claimed by Γ, possibly excluding the rather flexibly placeable compression chamber, to the structurable annular region spanning between $R_{\min}$ and $R_{\max}$. Figure 6c presents a structure Γ for which $\bar{A}$ (13) has been computationally minimized for $\Omega/2\pi = 25$ Hz, while, at the same time, a low band width $\Delta\Omega$ (7) is maintained. As the manufacturing tolerances $\{\Delta\gamma_k\}$

341   only account for a small fraction of the absolute dimensions of Γ, they do not substantially alter the
342   absolute and relative spatial footprints A_Γ and $\bar{A}$ (13), respectively. To reflect that central space is
343   most precious, a combination of the metrics $\bar{R}$ (11), $\check{R}$ (12) and $\bar{A}$ (13) may be employed for design
344   optimization of Γ.

Definition of Liquid Volumes

346   In centrifugally automated bioanalytical protocols, the precision $\Delta U_{0,i}$ of loaded liquid volumes $U_{0,i}$
347   by structures Γ_i directly enters mixing ratios of sample and reagents, and thus assay quantitation, as
348   well as valving performance in terms critical spin rates Ω (5), mostly through the radial product $\bar{r}\Delta r$
349   representing the spatial distribution $\Lambda = \Lambda(U_0)$. Uncertainties ΔU_0 in U_0 are generated during
350   introduction of the liquid into Γ through pipetting, and subsequent serial transfer through LUOs and
351   their valves before arriving in a final, end-point detection chamber.

352   Figure 7a reveals the significant growth of $\Delta\Omega$ with the spread ΔU_0 (with otherwise default tolerances
353   $\{\Delta\gamma_k\}$, see Appendix); the structure Γ in Figure 7b has been optimized to keep the standard deviation
354   $\Delta\Omega$ at bay for (rather large) $\Delta U_0 = 10$ µl.

| (a) $\Delta\Omega/2\pi$ vs. the standard deviation of the liquid volume ΔU_0 around $U_0 = 100$ µl loaded to the inlet of the base geometry Γ and default tolerances (see Appendix) with $\Omega/2\pi = 25$ Hz. | (b) Γ optimized for highest tolerance to (rather large) variations of loaded volume $\Delta U_0 = 10$ µl at $R = 3$ cm and $\Omega/2\pi = 25$ Hz with $\Delta\Omega/2\pi \approx 0.91$. |
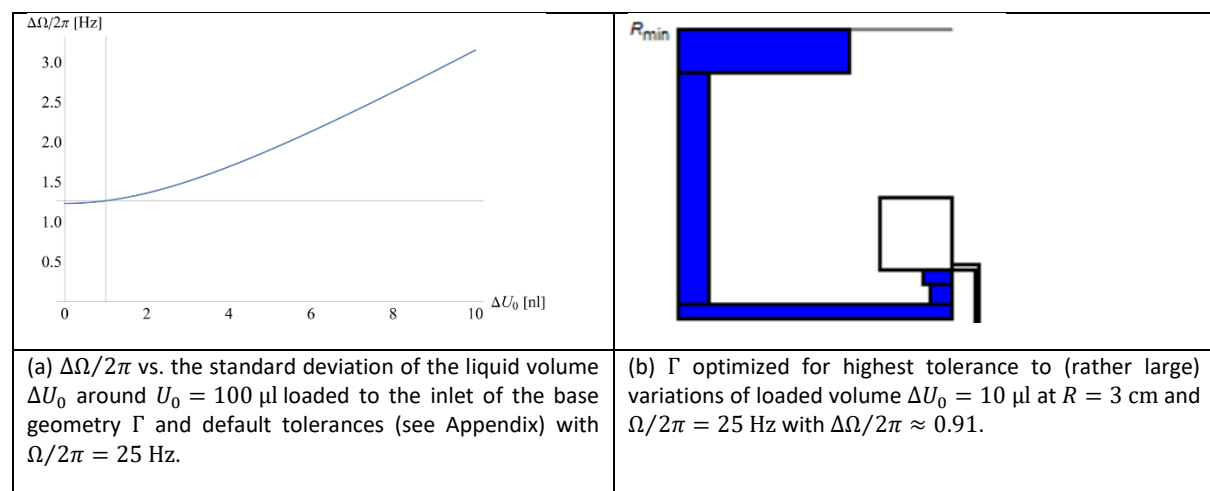
355   Figure 7 (a) Spread $\Delta\Omega$ as a function of the precision of the loaded volume ΔU_0 with default other values $\{\Delta\gamma_k\}$, with the
356   dotted lines representing the values used and obtained for the default parameters (see Appendix). (b) Structure Γ (excerpt)
357   optimized for minimum standard deviation $\Delta\Omega$ caused by a comparatively poor volume precision ΔU_0.

358   On the outlet side, valves retain a certain fraction of the introduced liquid volume U_0. While
359   reproducible losses U_{loss} may readily be compensated via the layout according to (5, 6), they tend to
360   raise space requirements; their impact can be mitigated through minimizing the metric

$$\bar{U}_{\mathrm{loss}} = \frac{U_{\mathrm{loss}}}{U_0} \approx \frac{d_0 \cdot w_0 \cdot (R - r_0) + U_{\mathrm{iso}} + d \cdot w \cdot Z}{U_0} \tag{14}$$

361   which assumes that the entire liquid filling Γ below its crest point R_{crest} will not be transferred upon
362   actuation in purely overflow driven CP-DF valving (see Figure 1 for parameter definitions).

363   Assuming that deviations from this model mainly result from pulley effects of the liquid plug of volume
364   $d \cdot w \cdot Z$ residing in the inbound segment (Figure 1), the metric

$$\overline{\Delta U}_{\mathrm{loss}} = \frac{\Delta U_{\mathrm{loss}}}{U_{\mathrm{loss}}} \approx \frac{d \cdot w \cdot Z}{d_0 \cdot w_0 \cdot (R - r_0) + U_{\mathrm{iso}} + d \cdot w \cdot Z} \tag{15}$$

365   accounts for its statistical variations ΔU_{loss} with respect to the total residual volume U_{loss}. The value
366   of $\overline{\Delta U}_{\mathrm{loss}}$ (15) should ideally vanish to minimize the band width $\Delta\Omega$ (7) and improve the related
367   bioanalytical precision, which is the case for merely overflow driven liquid transfer to the outer DF
368   chamber. Note that an experimental characterization or a refined, computational fluid dynamic (CFD)

369   simulation of the course of valving would be required to obtain a more accurate estimate of U_{loss} and
370   ΔU_{loss}.

Ambient Pressure

372   In the context of its definition, it was already reckoned that the rotationally induced pressure head p_ω
373   (1) only accounts for a smaller portion of the actual ambient pressure p_0. Therefore, the retention
374   rate $\Omega \propto \sqrt{p_0}$ (6) of centrifugo-pneumatic valves reacts rather sensitively to (typically slow) changes
375   of the atmospheric pressure p_0, e.g., caused by local altitude or weather. Figure 8a displays the shift
376   of the associated retention rate Ω over a range of typical, weather-related variations in p_0' of less than
377   4%. Even larger deviations are impacted with local altitude, roughly 10% per 1000 m. It therefore
378   makes sense to link a pressure sensor to a LoaD instrument in order to systematically adjust the spin
379   protocol $\omega(t)$ to the local ambient pressure p_0, which tends to stay fairly constant over the course of
380   an assay protocol, typically minutes to one hour.

381   Strictly speaking, formula (6) assumes that the ambient pressure p_0 is equal to the pressure of the air
382   entrapped in the compression chamber at the point of complete filling of the isoradial segment (Figure
383   1a). However, hydrodynamic effects might lead to deviations which we consider by extending (6)

$$\Omega = \sqrt{\frac{p_0 \cdot [(1 + \chi) \cdot V_{\text{C}}/V - 1]}{\varrho \cdot \bar{r}\Delta r}} \qquad (16)$$

384   with the unitless coefficient $\chi = p_0'/p_0 - 1$ reflecting the fractional divergence of the actual pressure
385   p_0' in the compression chamber at the point of pneumatic cut-off from the ambient pressure at p_0
386   (Figure 1a) [76]. Figure 8b shows that deviations $|\chi| > 0$, which are hard to measure experimentally,
387   should remain in the permille range, or at least be reproducible, i.e., $\Delta\chi \approx 0$, to allow proper
388   compensation for the shifts in the default retention rates $\{\Omega_i\}$ by modulating $\omega(t)$, to avoid having a
389   massive impact on the band width $\Delta\Omega$ (7).

(a) Variation of the retention rate Ω with the actual ambient p_0 near $p_{\text{std}} = 1013.25$ hPa.	(b) Variation of the retention rate Ω with $\chi = p_0'/p_0 - 1$ for changes up to about $\pm 1\%$.
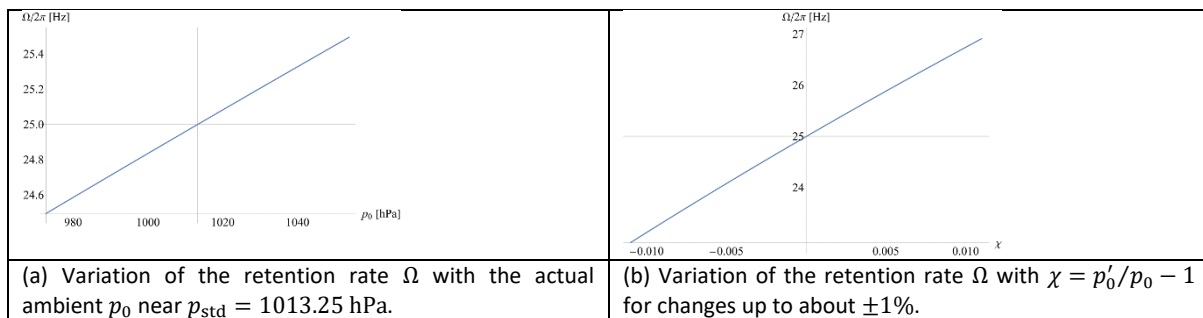
390   Figure 8 Variation of retention rate Ω vs (a) actual atmospheric pressure p_0 and (b) with the fractional deviation $\chi = p_0'/p_0 -$
391   1 of the pressure of the enclosed gas pocket p_0' from p_0 at the point of isolation from atmosphere (Figure 1a). Note that
392   variations in χ of more than a few permille have a considerable impact on Ω (5,6,16). The dotted lines indicate the standard
393   deviations $\Delta\Omega$ obtained at $p_0 = p_{\text{std}}$ (a) and for $\chi = 0$ (b) using the standard parameter values (see Appendix).

Manufacturing – Process Limitations and Costs

395   From a mere fluidic and mathematical point of view, elementary spatial needs may be captured rather
396   well by $\bar{R}$ (11), $\check{R}$ (12) and $\bar{A}$ (13). Yet, in practice, the degree of freedom in patterning structures Γ,
397   and their packing density empowering fluidic multiplexing, is further influenced by materials and their
398   processing technologies along prototyping, pilot series and (commercial) mass fabrication, the latter
399   being typically based on tool-based polymer replication and pick-and-place assembly schemes [83].

400   This repertoire of fabrication techniques commonly involves different dimensional tolerances, and
401   often imposes considerably varying types and magnitudes of design restrictions, e.g., on minimum
402   feature sizes, aspect ratios, wall thicknesses, draft angles (for demolding), the homogeneity of packing

403   density and the distribution of hydrodynamic resistances (for the flow of the mostly centrally,
404   pressure-injected hot melt), curvature of concave or convex edges on tools and their replicates, and
405   sufficient interstitial and peripheral surface area for pressure-proof bonding.

406   Furthermore, not all area untouched by Γ may be available for placing other structures, e.g., as it may
407   be too small or occluded in the center of a neighboring Γ. While these restrictions are hard to exactly
408   quantify, they might, more or less, be captured by a reserving a "fringe" of a width corresponding the
409   minimum wall thickness or bonding surface around the outer contours of Γ.

410   Thus, in addition to the fluidic aspects mostly addressed in this work, future endeavors should be
411   directed towards factoring in the design optimization towards criteria associated with manufacture
412   and assembly, and their effect on the technological challenge and related cost of development and
413   production [85].

Multi-Parameter Optimization

415   Given the complexity of these often somewhat conflicting design objectives, a multi-parameter
416   optimization usually needs to be implemented along the combined metric

$$\mathcal{M} = \sum_l c_l \cdot \mathcal{M}_l \tag{17}$$

417   to be computationally minimized. Each constituent $\mathcal{M}_l$ (17) is weighted by a numerical coefficient c_l,
418   optionally imposing normalization $\sum_l c_l = 1$. For instance, amongst the numerous possible scenarios,
419   a valving structure Γ may need to be geared to facilitate a certain (minimum) field strength f_ω (8)
420   while its band $\Omega \pm M \cdot \Delta\Omega$ (5) and radial extension $\bar{R}$ (11) need to fit into their still accessible corridors
421   in real and frequency space, respectively. Accordingly, the aggregate metric

$$\mathcal{M} = c_{f_\omega} \cdot \overline{f_\omega} + c_R \cdot \bar{R} + c_{\Delta\Omega} \cdot \overline{\Delta\Omega} \tag{18}$$

422   ought to be minimized within the available radial and frequency spaces, in the simplest case, with
423   equal coefficients $c_{f_\omega} = c_R = c_{\Delta\Omega} = 1/3$.

General Design Guidelines

425   Fitting a structure Γ into a given, still free "slot" in both, real and frequency space thus represents a
426   primary design goal directing the layout of multiplexed LoaD systems. Without a universal design
427   recipe owing to the plethora of possible application cases, a few important, partially counteracting
428   trends can still be pointed out.

429   The retention rate Ω (6) of a CP-DF siphon valve is chiefly affiliated with its radial position R and
430   geometry Γ, the liquid volume U_0 of density ϱ, and the ambient pressure p_0. Large Ω are achieved
431   towards high compression ratios V_C/V between the initial and final volumes of the entrapped gas,
432   and small radial products $\bar{r}\Delta r$. Consequently, high field strengths $f_\omega \propto R \cdot \Omega^2$ (8) at narrow $\Delta\Omega$ (Figure
433   2b) are best established at outer radial positions R.

434   The quotient V_C/V is directly related to the statically defined structure Γ. Moreover, the product $\bar{r}\Delta r$
435   immediately derives from the meniscus positions r_0 and r in the inlet reservoir and inbound segment,
436   respectively. In the general case, r_0 and r confining the liquid distribution Λ emerge in response to the
437   centrifugal, pneumatic and ambient pressures p_ω (1), p_V (2), and p_0. Yet, for $\omega = \Omega, r = R_{\text{crest}} = R -$
438   Z (Figure 1a), so r_0 becomes a function of Γ and U_0, and overall, $\Omega = \Omega(R, \Gamma, U_0, \varrho, p_0)$. The free
439   experimental parameters to set Ω are typically R, Γ and U_0, while ϱ is prescribed by the assay and p_0
440   by the local altitude, temperature and weather.

441   Furthermore, any tolerances $\Delta R, \Delta\Gamma, \Delta U_0, \Delta\varrho$ and Δp_0 in their corresponding input parameters
442   R, Γ, U_0, ϱ and p_0, and possibly $\chi \neq 0$ (16) echoing the filling dynamics, lead to a spread $\Delta\Omega$ in the

443   retention rate Ω. In most application setups, the actual ambient pressure $p_0 \neq p_{\text{std}}$ may be measured,
444   and remains reasonably constant over the course of a bioassay. Hence, statistical fluctuations Δp_0 can
445   be neglected, i.e., $\Delta p_0/p_0 \ll 1$, which can also be assumed for the density, i.e., $\Delta \varrho/\varrho \ll 1$.
446   Irreproducible filling procedures (Figure 1) can lead to statistical deviations $\Delta \chi \approx 0$, which may have
447   a significant impact on Ω (16) if exceeding the permille range (Figure 8b). Measures like slow, quasi-
448   static loading of the liquid, an optimized shape of the inlet reservoir and the tiny isoradial channel
449   imposing a significant hydrodynamic resistance to induce more reproducible laminar flow are thus
450   advisable.

451   If these considerations are considered, the standard deviation $\Delta \Omega$ mainly represents a function of the
452   pipetting precision ΔU_0 and the dimensional manufacturing tolerances $\{\Delta \gamma_k\}$ of Γ; importantly, these
453   variations are either well known from manuals or literature, or can rather easily be determined for a
454   particular material and its processing technique from comparatively simple, general-purpose test
455   structures, to generally inform $\Delta \Omega$ for a wide range of designs Γ. This way, the (costly) manufacture of
456   a large, statistically sufficient number of specific LoaD devices can be bypassed.

457   Restricting the band width $\Delta \Omega$ turns out to be particularly difficult towards large Ω. Figure 2 advises
458   that $\Delta \Omega$ reduces towards rising compression volumes V_C and outer radial positions R. This is reasoned
459   by the decreasing (relative) influence of manufacturing tolerances $\{\Delta \gamma_k\}$ defined on an absolute scale
460   towards growing structural dimensions of Γ. Furthermore, any deviations $\Delta \Gamma$ or ΔU_0 intimately affect
461   the magnitude of the radial product $\bar{r} \Delta r$. To stabilize both, $\bar{r}$ and Δr, the minimization of the band
462   width $\Delta \Omega$ thus typically involves widening of the radially inner segments near their meniscus positions
463   r_0 and R_{crest} assumed in the vicinity of the retention rate $\omega = \Omega$.

464   The results presented here for the optimizing valving structures Γ teach that the typical standard
465   deviation $\Delta \Omega$ of Ω ranges in the order of $\Delta \Omega/2\pi \approx 1 \text{ Hz}$. To assess the impact on robust fluidic
466   multiplexing, we consider the rotationally actuated serial release of N simultaneously loaded liquids,
467   with each valve operating at a component-level reliability $P_M = 99.99\%$ for $M = 4$; in this case, the
468   width of a band $\Omega \pm M \cdot \Delta \Omega$ calculates to $2 \cdot M \cdot \Delta \Omega \approx 8 \text{ Hz}$. Consequently, a frequency envelope
469   spanning over 40 Hz between $\omega_{\min}/2\pi = 15 \text{ Hz}$ and $\omega_{\max}/2\pi = 55 \text{ Hz}$ could, in theory, assure a
470   high system-level robustness of $P_{M=4}^N \approx 99.96\%$ for $N = 5$ independent, rotationally controllable
471   (high-pass) valves.

472   However, this envelope is often "squeezed" into upper regions of the frequency space, i.e., reducing
473   the frequency envelope $\omega'_{\min} \gg \omega_{\min}$. The new, higher boundary $\omega'_{\min}$ may be attributed to an LUO
474   occurring early in the liquid handling protocol of an assay, such as plasma separation, which would
475   require an inner position R of Γ, and thus a substantial critical spin rate $\Omega \gg \omega_{\min}$, to provide a
476   sufficient field strength f_ω (8) for guaranteeing swift and high-quality sedimentation. All
477   simultaneously loaded, and later opened high-pass valves would, accordingly, must accommodate
478   their bands in this much narrower, upper frequency corridor.

Summary and Outlook

480   Large-scale integration (LSI) of fluidic networks constitutes a key prerequisite for comprehensive
481   sample-to-answer automation of parallelized, multi-step / multi-reagent bioassay protocols suitable
482   for application at the Point-of-Care or Point-of-Use. A powerful digital twin concept was elaborated
483   for conceptually simple, rotationally actuated flow control by centrifugo-pneumatic dissolvable-film
484   (CP-DF) siphon valves on "Lab-on-a-Disc" systems operating in batch-mode; to accomplish high
485   functional packing density without sacrificing commercially critical operational robustness, it was
486   shown that, in addition the spatial footprint and radial placement, mainly the minimization of the

487   standard deviation $\Delta\Omega$ arising from the limited precision of experimental input parameters assumes a
488   crucial role.

489   Performance goals were achieved by (computationally) minimization a suite of distinct performance
490   metrics over the multiparameter space of exemplary, highly configurable CP-DF siphon valves. The
491   model-based approach offers a viable alternative to lengthy and expensive manufacture and
492   experimental characterization at system level, which requires device numbers and testing facilities
493   that are largely unavailable at the development stage and along scale-up using different
494   manufacturing techniques.

495   It is to mention that, alternatively to fluidic LSI, multiplexed detection has also been achieved through
496   other schemes such as bead-based or label-based methods, sometimes in combination with off-chip
497   sample preconditioning or detection. A thorough investigation of their pros and cons turns out to be
498   highly application-specific, and falls beyond the scope of this research article. Generally speaking, such
499   substitutional, bead- or label-based methods require common assay chemistries for all analytes, and
500   rather complex optical encoding or multi-wavelength readout; these enhanced technical demands
501   need to comply with the cost base and ruggedness of the instrument for its deployment outside
502   professional environments, and for markedly lower throughputs characteristic for decentralized
503   deployment, e.g., in patient self-testing at home.

504   Future work should include more complex geometries, and elastic elements in the fluidic modelling,
505   e.g., reflecting the bending of lids, compression and friction of trapped gas bubbles, and hydrodynamic
506   effects, thus sophisticating design rules with even higher predictability of performance and reliability.
507   The modelling should also incorporate other, especially rotationally actuated valving and flow control
508   techniques. To create more disc space, options of multilayer stacking may be explored. Disc designs
509   may also contain anti-counterfeit features based on superior control of manufacture and its
510   tolerances, or secret fluidic "key codes" that can be flexibly defined at the factory [86].

511   In addition, simulation of fabrication processes and assay kinetics would clearly augment the digital
512   twin approach. Eventually, professional layout software may be provided, which would, for instance,
513   enable foundry services as a landmark of mature supply chains. Regarding the bigger picture, the
514   publication of the digital twin can set the stage for open platform models that have already been
515   discussed in the context of crowdsourcing, e.g., through blockchain-backed, participatory research
516   models [87-90].

Appendix: Default Valve Geometry

518   The structure Γ, their radial positions R and loaded by liquid volumes U_0 can be varied across a multi-
519   dimensional parameter space, e.g., to tune retention rates Ω, or other key performance indicators.
520   Table A1 provides of overview or generic values for the parameters displayed in Figure 1 which can be
521   used to initiate design optimization according to the metrics $\{\mathcal{M}_l\}$.

$R = 3$ cm	$R_{\min} = 1.5$ cm	$R_{\max} = 5.5$ cm	$R_{DF} = 3.15$ cm $> R$
$A_0 = d_0 \cdot w_0$	$d_0 = 1$ mm	$w_0 = 5$ mm	
$U_0 = 100$ μl $< A_0 \cdot (R - R_{\min})$			
$U_{iso} = d_0 \cdot h \cdot L \ll U_0$	$d_{iso} = 1$ mm	$h_{iso} = 1$ mm	$L_{iso} = 15$ mm $> w_0 + w$
$U_Z = d \cdot w \cdot Z$	$d = 500$ μm	$w = 800$ μm $\ll w_0$	$Z = 10$ mm
$V_{C,0} = d_C \cdot w_C \cdot h_C \gg U_Z$	$d_C = 1$ mm	$w_C = 20$ mm	$h_C = 10$ mm
$V_{int} = d_{int} \cdot h_{int} \cdot L_{int} \ll V_C$	$d_{int} = 200$ μm	$h_{int} = 300$ μm	$L_{int} = 1$ cm $> 2w$
$V_{DF} = 0.25\pi \cdot d_{DF} \cdot D_{DF}^2 \ll V_C$	$d_{DF} = 190$ μm	$D_{DF} = 3$ mm	$\alpha = 0.45, \beta = 0.5$

522   Table A1 Default geometrical parameters and relationships of basic CP-DF siphon valves (Figure 1). The resulting critical spin
523   rate $\Omega(R, \Gamma, U_0)/2\pi \approx 25$ Hz. Minimum lateral dimensions are given by the smallest practical diameter of milling tools (200

524 μm). As tools for injection molding are often adopted from optical data storage (e.g., CD, DVD, Blu-ray), a central, 1.5-cm
525 diameter hole and a disc radius of 6 cm with thickness around 1.2 mm, fluidic structures Γ may need to stay within the radial
526 interval between $R_{\min} = 1.5$ cm and $R_{\max} = 5.5$ cm, and an upper limit for the depth of about 1 mm, as chosen for the
527 main parts of geometries Γ. For large lateral extensions or small aspect ratios, sagging of the lid, which is often provided by
528 a rather flexible foil, may significantly alter the nominal volume capacity, also in response to the pressure, and might even
529 lead to sticking to the bottom of the cavity.

530 The default tolerances $\Delta\gamma_k$ in the chief input parameters γ_k are:

531 • Lateral structuring $\Delta w = \Delta h = 20$ μm
532 • Vertical structuring $\Delta d = 30$ μm
533 • Precision of liquid volume $\Delta U_0/U_0 = 1\%$
534 • Ambient pressure $\Delta p_0 = 40$ hPa

535 In the digital twin model, different standard deviations $\{\Delta\gamma_k\}$ may easily be plugged into the
536 calculations.

References

538 1. Manz, A., N. Graber, and H.M. Widmer *Miniaturized total chemical analysis systems: A novel
539 concept for chemical sensing*. Sensors and Actuators B: Chemical, 1990. **1**, 244-248 DOI:
540 10.1016/0925-4005(90)80209-I.
541 2. Reyes, D.R., D. Iossifidis, P.-A. Auroux, and A. Manz *Micro Total Analysis Systems. 1.
542 Introduction, Theory, and Technology*. Analytical Chemistry, 2002. **74**, 2623-2636 DOI:
543 10.1021/ac0202435.
544 3. Auroux, P.-A., D. Iossifidis, D.R. Reyes, and A. Manz *Micro Total Analysis Systems. 2. Analytical
545 Standard Operations and Applications*. Analytical Chemistry, 2002. **74**, 2637-2652 DOI:
546 10.1021/ac020239t.
547 4. Whitesides, G.M. *The origins and the future of microfluidics*. Nature, 2006. **442**, 368-373 DOI:
548 10.1038/nature05058.
549 5. Craighead, H., *Future lab-on-a-chip technologies for interrogating individual molecules.*
550 Nature, 2006. **442**(7101): p. 387-93.
551 6. El-Ali, J., P.K. Sorger, and K.F. Jensen, *Cells on chips.* Nature, 2006. **442**(7101): p. 403-11.
552 7. Janasek, D., J. Franzke, and A. Manz, *Scaling and the design of miniaturized chemical-analysis
553 systems.* Nature, 2006. **442**(7101): p. 374-80.
554 8. Schembri, C.T., V. Ostoich, P.J. Lingane, T.L. Burd, and S.N. Buhl *Portable Simultaneous
555 Multiple Analyte Whole-Blood Analyzer for Point-of-Care Testing*. Clinical Chemistry, 1992. **38**,
556 1665-1670 DOI: 10.1093/clinchem/38.9.1665.
557 9. Schembri, C.T., T.L. Burd, A.R. Kopfsill, L.R. Shea, and B. Braynin *Centrifugation and Capillarity
558 Integrated into a Multiple Analyte Whole-Blood Analyzer*. Journal of Automatic Chemistry,
559 1995. **17**, 99-104 DOI: 10.1155/S1463924695000174.
560 10. *Abaxis*. Available on: https://www.abaxis.com/.
561 11. Andersson, P., G. Jesson, G. Kylberg, G. Ekstrand, and G. Thorsen *Parallel nanoliter microfluidic
562 analysis system*. Analytical Chemistry, 2007. **79**, 4022-4030 DOI: 10.1021/ac061692y.
563 12. Inganas, M., H. Derand, A. Eckersten, G. Ekstrand, A.K. Honerud, G. Jesson, G. Thorsen, T.
564 Soderman, and P. Andersson *Integrated microfluidic compact disc device with potential use in
565 both centralized and point-of-care laboratory settings*. Clinical Chemistry, 2005. **51**, 1985-7
566 DOI: 10.1373/clinchem.2005.053181.
567 13. *Gyros Protein Technologies*. Available on: https://www.gyrosproteintechnologies.com/.
568 14. Madou, M.J. and G.J. Kellogg *The LabCD (TM): A centrifuge-based microfluidic platform for
569 diagnostics*. Systems and Technologies for Clinical Diagnostics and Drug Discovery,
570 Proceedings Of, 1998. **3259**, 80-93 DOI: 10.1117/12.307314.

15. Shea, M. *ADMET Assays on Tecan's LabCD-ADMET System*. Journal of the Association for Laboratory Automation, 2003. **8**, 74-77 DOI: 10.1016/s1535-5535(04)00260-6.

16. Smith, S., D. Mager, A. Perebikovsky, E. Shamloo, D. Kinahan, R. Mishra, S.M.T. Delgado, H. Kido, S. Saha, J. Ducrée, M. Madou, K. Land, and J.G. Korvink *CD-Based Microfluidics for Primary Care in Extreme Point-of-Care Settings*. Micromachines, 2016. **7**, DOI: 10.3390/mi7020022.

17. Kong, L.X., A. Perebikovsky, J. Moebius, L. Kulinsky, and M. Madou *Lab-on-a-CD: A Fully Integrated Molecular Diagnostic System*. Journal of the Association for Laboratory Automation, 2016. **21**, 323-355 DOI: 10.1177/2211068215588456.

18. Maguire, I., R. O'Kennedy, J. Ducrée, and F. Regan *A review of centrifugal microfluidics in environmental monitoring*. Analytical Methods, 2018. **10**, 1497-1515 DOI: 10.1039/c8ay00361k.

19. Gorkin, R., J. Park, J. Siegrist, M. Amasia, B.S. Lee, J.M. Park, J. Kim, H. Kim, M. Madou, and Y.K. Cho *Centrifugal microfluidics for biomedical applications*. Lab on a Chip, 2010. **10**, 1758-1773 DOI: 10.1039/b924109d.

20. Burger, R., L. Amato, and A. Boisen *Detection methods for centrifugal microfluidic platforms*. Biosensors and Bioelectronics, 2016. **76**, 54-67 DOI: 10.1016/j.bios.2015.06.075.

21. Ducrée, J., S. Haeberle, S. Lutz, S. Pausch, F. von Stetten, and R. Zengerle *The centrifugal microfluidic Bio-Disk platform*. Journal of Micromechanics and Microengineering, 2007. **17**, S103-S115 DOI: 10.1088/0960-1317/17/7/S07.

22. Lutz, S., D. Mark, G. Roth, R. Zengerle, and F. von Stetten, *Centrifugal Microfluidic Platforms for Molecular Diagnostics.* Clinical Chemistry and Laboratory Medicine, 2011. **49**: p. S608-S608.

23. Tang, M., G. Wang, S.-K. Kong, and H.-P. Ho *A Review of Biomedical Centrifugal Microfluidic Platforms*. Micromachines, 2016. **7**, DOI: 10.3390/mi7020026.

24. Duffy, D.C., H.L. Gillis, J. Lin, N.F. Sheppard, and G.J. Kellogg *Microfabricated Centrifugal Microfluidic Systems: Characterization and Multiple Enzymatic Assays*. Analytical Chemistry, 1999. **71**, 4669-4678 DOI: 10.1021/ac990682c.

25. Azimi-Boulali, J., M. Madadelahi, M.J. Madou, and S.O. Martinez-Chapa *Droplet and Particle Generation on Centrifugal Microfluidic Platforms: A Review*. Micromachines, 2020. **11**, DOI: 10.3390/mi11060603.

26. Tang, M., G. Wang, S.K. Kong, and H.P. Ho *A Review of Biomedical Centrifugal Microfluidic Platforms*. Micromachines, 2016. **7**, DOI: 10.3390/mi7020026.

27. Strohmeier, O., M. Keller, F. Schwemmer, S. Zehnle, D. Mark, F. von Stetten, R. Zengerle, and N. Paust *Centrifugal microfluidic platforms: advanced unit operations and applications*. Chemical Society Reviews, 2015. **44**, 6187-229 DOI: 10.1039/c4cs00371c.

28. Kong, L.X., A. Perebikovsky, J. Moebius, L. Kulinsky, and M. Madou *Lab-on-a-CD*. Journal of Laboratory Automation, 2016. **21**, 323-355 DOI: 10.1177/2211068215588456.

29. Aeinehvand, M.M., P. Magaña, M.S. Aeinehvand, O. Aguilar, M.J. Madou, and S.O. Martinez-Chapa *Ultra-rapid and low-cost fabrication of centrifugal microfluidic platforms with active mechanical valves*. RSC Advances, 2017. **7**, 55400-55407 DOI: 10.1039/c7ra11532f.

30. Aeinehvand, M.M., L. Weber, M. Jiménez, A. Palermo, M. Bauer, F.F. Loeffler, F. Ibrahim, F. Breitling, J. Korvink, M. Madou, D. Mager, and S.O. Martínez-Chapa *Elastic reversible valves on centrifugal microfluidic platforms*. Lab on a Chip, 2019. **19**, 1090-1100 DOI: 10.1039/C8LC00849C.

31. Hess, J.F., S. Zehnle, P. Juelg, T. Hutzenlaub, R. Zengerle, and N. Paust *Review on pneumatic operations in centrifugal microfluidics*. Lab on a Chip, 2019. **19**, 3745-3770 DOI: 10.1039/C9LC00441F.

32. Nguyen, H.V., V.D. Nguyen, H.Q. Nguyen, T.H.T. Chau, E.Y. Lee, and T.S. Seo *Nucleic acid diagnostics on the total integrated lab-on-a-disc for point-of-care testing*. Biosensors and Bioelectronics, 2019. **141**, 111466 DOI: 10.1016/j.bios.2019.111466.

33. Rombach, M., S. Hin, M. Specht, B. Johannsen, J. Lüddecke, N. Paust, R. Zengerle, L. Roux, T. Sutcliffe, J.R. Peham, C. Herz, M. Panning, O. Donoso Mantke, and K. Mitsakakis *RespiDisk: a point-of-care platform for fully automated detection of respiratory tract infection pathogens in clinical samples*. The Analyst, 2020. **145**, 7040-7047 DOI: 10.1039/d0an01226b.

34. Homann, A.R., L. Niebling, S. Zehnle, M. Beutler, L. Delamotte, M.-C. Rothmund, D. Czurratis, K.-D. Beller, R. Zengerle, H. Hoffmann, and N. Paust *A microfluidic cartridge for fast and accurate diagnosis of Mycobacterium tuberculosis infections on standard laboratory equipment*. Lab on a Chip, 2021. DOI: 10.1039/d1lc00035g.

35. Madadelahi, M., L.F. Acosta-Soto, S. Hosseini, S.O. Martinez-Chapa, and M.J. Madou *Mathematical modeling and computational analysis of centrifugal microfluidic platforms: a review*. Lab on a Chip, 2020. **20**, 1318-1357 DOI: 10.1039/c9lc00775j.

36. Miyazaki, C.M., E. Carthy, and D.J. Kinahan *Biosensing on the Centrifugal Microfluidic Lab-on-a-Disc Platform*. Processes, 2020. **8**, 1360 DOI: 10.3390/pr8111360.

37. Rombach, M., S. Hin, M. Specht, B. Johannsen, J. Lüddecke, N. Paust, R. Zengerle, L. Roux, T. Sutcliffe, J.R. Peham, C. Herz, M. Panning, O. Donoso Mantke, and K. Mitsakakis, *RespiDisk: a point-of-care platform for fully automated detection of respiratory tract infection pathogens in clinical samples.* The Analyst, 2020. **145**(21): p. 7040-7047.

38. *Gamera Bioscience Corp. [acquired by Tecan]*.

39. *Burstein Technologies, Inc. [archived]*. 2006; Accessed: 31/05/2021; Available on: https://web.archive.org/web/20061209052345/http://www.bursteintechnologies.com.

40. *Biosurfit SA*. Available on: https://www.biosurfit.com/.

41. *Spindiag GmbH*. Available on: http://www.spindiag.de.

42. *RotaPrep Inc.*; Accessed: 19/04/2021; Available on: https://rotaprep.com/.

43. *LaMotte Chemical Products Co*. Available on: https://www.lamotte.com.

44. *Radisens Diagnostics*. Available on: www.radisens.com.

45. *Blusense Diagnostics*. Available on: https://blusense-diagnostics.com/.

46. *SpinX Technologies*. Available on: http://www.spinx-technologies.com.

47. Clime, L., J. Daoud, D. Brassard, L. Malic, M. Geissler, and T. Veres *Active pumping and control of flows in centrifugal microfluidics*. Microfluidics and Nanofluidics, 2019. **23**, DOI: 10.1007/s10404-019-2198-x.

48. Brassard, D., M. Geissler, M. Descarreaux, D. Tremblay, J. Daoud, L. Clime, M. Mounier, D. Charlebois, and T. Veres *Extraction of nucleic acids from blood: unveiling the potential of active pneumatic pumping in centrifugal microfluidics for integration and automation of sample preparation processes*. Lab on a Chip, 2019. **19**, 1941-1952 DOI: 10.1039/c9lc00276f.

49. Abi-Samra, K., R. Hanson, M. Madou, and R.A. Gorkin *Infrared controlled waxes for liquid handling and storage on a CD-microfluidic platform*. Lab on a Chip, 2011. **11**, 723-726 DOI: 10.1039/c0lc00160k.

50. Kong, L.X., K. Parate, K. Abi-Samra, and M. Madou *Multifunctional wax valves for liquid handling and incubation on a microfluidic CD*. Microfluidics and Nanofluidics, 2015. **18**, 1031-1037 DOI: 10.1007/s10404-014-1492-x.

51. Torres Delgado, S.M., D.J. Kinahan, L.A. Nirupa Julius, A. Mallette, D.S. Ardila, R. Mishra, C.M. Miyazaki, J.G. Korvink, J. Ducrée, and D. Mager *Wirelessly powered and remotely controlled valve-array for highly multiplexed analytical assay automation on a centrifugal microfluidic platform*. Biosensors and Bioelectronics, 2018. **109**, 214-223 DOI: 10.1016/j.bios.2018.03.012.

52. Kinahan, D.J., M. Renou, D. Kurzbuch, N.A. Kilcawley, E. Bailey, M.T. Glynn, C. McDonagh, and J. Ducrée *Baking Powder Actuated Centrifugo-Pneumatic Valving for Automation of Multi-Step Bioassays*. Micromachines, 2016. **7**, DOI: 10.3390/mi7100175.

53. Haeberle, S., T. Brenner, R. Zengerle, and J. Ducrée *Centrifugal extraction of plasma from whole blood on a rotating disk*. Lab on a Chip, 2006. **6**, 776-781 DOI: 10.1039/b604145k.

671   54.   Steigert, J., T. Brenner, M. Grumann, L. Riegger, S. Lutz, R. Zengerle, and J. Ducrée *Integrated*
672   *siphon-based metering and sedimentation of whole blood on a hydrophilic lab-on-a-disk*.
673   Biomedical Microdevices, 2007. **9**, 675-679 DOI: 10.1007/s10544-007-9076-0.
674   55.   Kinahan, D.J., S.M. Kearney, N.A. Kilcawley, P.L. Early, M.T. Glynn, and J. Ducrée *Density-*
675   *Gradient Mediated Band Extraction of Leukocytes from Whole Blood Using Centrifugo-*
676   *Pneumatic Siphon Valving on Centrifugal Microfluidic Discs*. PLOS ONE, 2016. **11**, e0155545
677   DOI: 10.1371/journal.pone.0155545.
678   56.   Dimov, N., J. Gaughran, D. Mc Auley, D. Boyle, D.J. Kinahan, and J. Ducrée *Centrifugally*
679   *Automated Solid-Phase Purification of RNA*. 2014 IEEE 27th International Conference on Micro
680   Electro Mechanical Systems (MEMS), 2014. 260-263 DOI: 10.1109/MEMSYS.2014.6765625.
681   57.   Gaughran, J., D. Boyle, J. Murphy, R. Kelly, and J. Ducrée *Phase-selective graphene oxide*
682   *membranes for advanced microfluidic flow control*. Microsystems and Nanoengineering,
683   2016. **2**, 16008 DOI: 10.1038/micronano.2016.8.
684   58.   Zehnle, S., M. Rombach, R. Zengerle, F. von Stetten, and N. Paust *Network simulation-based*
685   *optimization of centrifugopneumatic blood plasma separation*. Biomicrofluidics, 2017. **11**,
686   DOI: 10.1063/1.4979044.
687   59.   Al-Faqheri, W., T.H.G. Thio, M.A. Qasaimeh, A. Dietzel, M. Madou, and A. Al-Halhouli,
688   *Particle/cell separation on microfluidic platforms based on centrifugation effect: a review.*
689   Microfluidics and Nanofluidics, 2017. **21**(6).
690   60.   Mark, D., S. Haeberle, T. Metz, S. Lutz, J. Ducrée, R. Zengerle, and F. von Stetten *Aliquoting*
691   *structure for centrifugal microfluidics based on a new pneumatic valve*. MEMS 2008: 21st Ieee
692   International Conference on Micro Electro Mechanical Systems, Technical Digest, 2008. 611-
693   +.
694   61.   Schwemmer, F., T. Hutzenlaub, D. Buselmeier, N. Paust, F. von Stetten, D. Mark, R. Zengerle,
695   and D. Kosse *Centrifugo-pneumatic multi-liquid aliquoting-parallel aliquoting and*
696   *combination of multiple liquids in centrifugal microfluidics*. Lab on a Chip, 2015. **15**, 3250-3258
697   DOI: 10.1039/c5lc00513b.
698   62.   Keller, M., S. Wadle, N. Paust, L. Dreesen, C. Nuese, O. Strohmeier, R. Zengerle, and F. von
699   Stetten *Centrifugo-thermopneumatic fluid control for valving and aliquoting applied to*
700   *multiplex real-time PCR on off-the-shelf centrifugal thermocycler*. RSC Advances, 2015. **5**,
701   89603-89611 DOI: 10.1039/c5ra16095b.
702   63.   Grumann, M., A. Geipel, L. Riegger, R. Zengerle, and J. Ducrée *Batch-mode mixing on*
703   *centrifugal microfluidic platforms*. Lab on a Chip, 2005. **5**, 560-5 DOI: 10.1039/b418253g.
704   64.   Ducrée, J., T. Brenner, S. Haeberle, T. Glatzel, and R. Zengerle *Multilamination of flows in*
705   *planar networks of rotating microchannels*. Microfluidics and Nanofluidics, 2006. **2**, 78-84 DOI:
706   10.1007/s10404-005-0056-5.
707   65.   Burger, R., D. Kinahan, H. Cayron, N. Reis, J. Garcia da Fonseca, and J. Ducrée *Siphon-induced*
708   *droplet break-off for enhanced mixing on a centrifugal platform*. Inventions, 2020. **5**, DOI:
709   10.3390/inventions5010001.
710   66.   Ducrée, J., S. Haeberle, T. Brenner, T. Glatzel, and R. Zengerle *Patterning of flow and mixing in*
711   *rotating radial microchannels*. Microfluidics and Nanofluidics, 2006. **2**, 97-105 DOI:
712   10.1007/s10404-005-0049-4.
713   67.   Strohmeier, O., S. Keil, B. Kanat, P. Patel, M. Niedrig, M. Weidmann, F. Hufert, J. Drexler, R.
714   Zengerle, and F. von Stetten *Automated nucleic acid extraction from whole blood, B. subtilis,*
715   *E. coli, and Rift Valley fever virus on a centrifugal microfluidic LabDisk*. RSC Advances, 2015. **5**,
716   32144-32150 DOI: 10.1039/c5ra03399c.
717   68.   Karle, M., J. Miwa, G. Roth, R. Zengerle, and F. von Stetten *A Novel Microfluidic Platform for*
718   *Continuous DNA Extraction and Purification Using Laminar Flow Magnetophoresis*. IEEE 22nd
719   International Conference on Micro Electro Mechanical Systems (MEMS 2009), 2009. 276-279
720   DOI: 10.1109/Memsys.2009.4805372.

69. Kido, H., M. Micic, D. Smith, J. Zoval, J. Norton, and M. Madou *A novel, compact disk-like centrifugal microfluidics system for cell lysis and sample homogenization*. Colloids and Surfaces B-Biointerfaces, 2007. **58**, 44-51 DOI: 10.1016/j.colsurfb.2007.03.015.

70. Haeberle, S., R. Zengerle, and J. Ducrée *Centrifugal generation and manipulation of droplet emulsions*. Microfluidics and Nanofluidics, 2007. **3**, 65-75 DOI: 10.1007/s10404-006-0106-7.

71. Schuler, F., F. Schwemmer, M. Trotter, S. Wadle, R. Zengerle, F. von Stetten, and N. Paust *Centrifugal step emulsification applied for absolute quantification of nucleic acids by digital droplet RPA*. Lab on a Chip, 2015. **15**, 2759-2766 DOI: 10.1039/c5lc00291e.

72. Schuler, F., M. Trotter, M. Geltman, F. Schwemmer, S. Wadle, E. Dominguez-Garrido, M. Lopez, C. Cervera-Acedo, P. Santibanez, F. von Stetten, R. Zengerle, and N. Paust *Digital droplet PCR on disk*. Lab on a Chip, 2016. **16**, 208-216 DOI: 10.1039/c5lc01068c.

73. Brennan, D., H. Coughlan, E. Clancy, N. Dimov, T. Barry, D. Kinahan, J. Ducrée, T.J. Smith, and P. Galvin *Development of an on-disc isothermal in vitro amplification and detection of bacterial RNA*. Sensors and Actuators, B: Chemical, 2017. **239**, 235-242 DOI: 10.1016/j.snb.2016.08.018.

74. Delgado, S.M.T., D.J. Kinahan, F.S. Sandoval, L.A.N. Julius, N.A. Kilcawley, J. Ducrée, and D. Mager *Fully automated chemiluminescence detection using an electrified-Lab-on-a-Disc (eLoaD) platform*. Lab on a Chip, 2016. **16**, 4002-4011 DOI: 10.1039/c6lc00973e.

75. Zehnle, S., F. Schwemmer, R. Bergmann, F. von Stetten, R. Zengerle, and N. Paust *Pneumatic siphon valving and switching in centrifugal microfluidics controlled by rotational frequency or rotational acceleration*. Microfluidics and Nanofluidics, 2015. **19**, 1259-1269 DOI: 10.1007/s10404-015-1634-9.

76. Ducrée, J. *Systematic review of centrifugal valving based on digital twin modelling towards highly integrated Lab-on-a-Disc systems*. Nature Microsystems & Nanoengineering, 2021. DOI: 10.20944/preprints202105.0683.v1.

77. Zehnle, S., M. Rombach, R. Zengerle, F. von Stetten, and N. Paust, *Network simulation-based optimization of centrifugo-pneumatic blood plasma separation.* Biomicrofluidics, 2017. **11**(2).

78. *Digital Twin*. 2021; Accessed: 25/05/2021; Available on: https://en.wikipedia.org/wiki/Digital_twin.

79. Marr, B. *What Is Digital Twin Technology - And Why Is It So Important?* 2017 Published: 06/03/2017; Accessed: 25/05/2021; Available on: https://www.forbes.com/sites/bernardmarr/2017/03/06/what-is-digital-twin-technology-and-why-is-it-so-important/.

80. Grieves, M. and J. Vickers, *Digital Twin: Mitigating Unpredictable, Undesirable Emergent Behavior in Complex Systems*, in *Transdisciplinary Perspectives on Complex Systems: New Findings and Approaches*, F.-J. Kahlen, S. Flumerfelt, and A. Alves, Editors. 2017, Springer International Publishing: Cham. p. 85-113.

81. Thorsen, T., *Microfluidic Large-Scale Integration.* Science, 2002. **298**(5593): p. 580-584.

82. Ducrée, J. *Secure air traffic control at the hub of multiplexing on the centrifugo-pneumatic Lab-on-a-Disc platform*. Micromachines, 2021. DOI: 10.20944/preprints202104.0612.v1

83. Ducrée, J. *Efficient development of integrated Lab-On-A-Chip systems featuring operational robustness and nanufacturability*. Micromachines, 2019. **10**, 12 DOI: 10.3390/mi10120886.

84. Reyes, D.R., H.v. Heeren, S. Guha, L.H. Herbertson, A.P. Tzannis, J. Ducrée, H. Bissig, and H. Becker *Accelerating Innovation and Commercialization Through Standardization of Microfluidic-Based Medical Devices*. Lab on a Chip, 2021. **21**, 9-21 DOI: 10.1039/D0LC00963F.

85. Ducrée, J. *Efficient Development of Microfluidic Solutions for Bioanalytical "Point-of-Use" Testing towards High-Technology-Readiness Levels—A Platform-Based Design-for-Manufacture Approach*. Proceedings, 2019. **2**, DOI: 10.3390/proceedings2131097.

86. Ducrée, J. *Anti-counterfeit technologies for centrifugal microfluidic "Lab-on-a-Disc" systems: An analysis*. 2021.

87. Ducrée, J., M. Etzrodt, S. Bartling, R. Walshe, T. Harrington, N. Wittek, S. Posth, K. Wittek, A. Ionita, W. Prinz, and J. Lawton *Unchaining Collective Intelligence for Science, Research and*

772   *Technology Development by Blockchain-Boosted Community Participation*. Frontiers in
773   Blockchain, 2020. **4**, 631648 DOI: 10.3389/fbloc.2021.631648.
774 88. Ducrée, J. *Research – A blockchain of knowledge?* Blockchain: Research and Applications,
775   2020. **1**, 100005 DOI: 10.1016/j.bcra.2020.100005.
776 89. Ducrée, J., M. Gravitt, R. Walshe, S. Bartling, M. Etzrodt, and T. Harrington *Open Platform*
777   *Concept for Blockchain-Enabled Crowdsourcing of Technology Development and Supply*
778   *Chains*. Frontiers in Blockchain, 2020. **3**, 386525 DOI: 10.3389/fbloc.2020.586525.
779 90. Ducrée, J., M. Etzrodt, B. Gordijn, M. Gravitt, S. Bartling, R. Walshe, and T. Harrington
780   *Blockchain for Organising Effective Grass-Roots Actions on a Global Commons: Saving The*
781   *Planet*. Frontiers in Blockchain, 2020. **3**, 33 DOI: 10.3389/fbloc.2020.00033.

782